Imaging entanglement correlations with a single-photon avalanche diode camera

Bienvenu Ndagano,[1,*] Hugo Defienne,[1] Ashley Lyons,[1] Ilya Starshynov,[1] Federica Villa,[2] Simone Tisa,[3] and Daniele Faccio[1,†]

[1]*School of Physics and Astronomy, University of Glasgow, Glasgow G12 8QQ, UK*
[2]*Politecnico di Milano, Dipartimento di Elettronica, Informazione e Bioingegneria, Piazza Leonardo da Vinci 32, 20133, Milano, Italy*
[3]*Micro Photon Device SRL, Via Waltraud Gebert Deeg 3g, I-39100, Bolzano, Italy*

(Dated: January 24, 2020)

Spatial correlations between two photons are the key resource in realising many quantum imaging schemes. Measurement of the bi-photon correlation map is typically performed using single-point scanning detectors or single-photon cameras based on CCD technology. However, both approaches are limited in speed due to the slow scanning and the low frame-rate of CCD-based cameras, resulting in data acquisition times on the order of many hours. Here we employ a high frame rate, single photon avalanche diode (SPAD) camera, to measure the spatial joint probability distribution of a bi-photon state produced by spontaneous parametric down-conversion, with statistics taken over 10^7 frames acquired in just 140 seconds. We verified the presence of spatial entanglement between our photon pairs through the violation of an Einstein-Podolsky-Rosen criterion, with a confidence level of 227 sigmas. Our work demonstrates the potential of SPAD cameras in the rapid characterisation of photon correlations, leading the way towards quantum imaging in real-time.

I. INTRODUCTION

Individual single photon avalanche diodes (SPADs) have long been the workhorse of many quantum optics experiments[1,2]. This is due largely to their single photon level sensitivity, and also to the Geiger mode operation which allows for straightforward methods of single photon discrimination and counting, provided the detector operates in the photon-starved regime. Furthermore, the presence of quenching electronics results in an impulse response function (IRF) that can be as short as 20 ps[3], which is ideal for measuring temporal correlations between multiple photons whilst reducing the influence of background radiation and dark counts. These properties make SPADs one of the leading technologies for measuring photon-photon correlations and entanglement.

Arrays of SPADs, or SPAD cameras, fabricated with standard CMOS technology, have been produced in recent years and are now commercially available (e.g. from Photon Force, Micro Photon Devices). The maturity of the technology has enabled the production of compact arrays[4,5], as well as the reduction of the cost per device through bulk manufacturing processes[6]. Thus far, imaging devices based on SPADs have demonstrated their capabilities in fluorescence lifetime imaging[6–8], LiDAR[9–12], non-line-of-sight imaging[13], and imaging through strongly scattering media[14]. However, SPAD cameras have yet to make their mark due to their overall efficiency and resolution; the fill-factor of the earliest available SPAD cameras was on the order of a few percent[6,15] which, despite the quantum efficiency of the single SPAD pixels being on par with commercial single element SPADs, equates to a large loss of the device overall. This high loss is particularly detrimental to the detection of quantum states formed of multiple photons as it scales with the power of the photon number.

CCD based single photon cameras have therefore been typically preferred for quantum imaging applications, where one of the routine tasks involves measuring spatial correlations between photons to build an image. This in turn is a result of the photon source of choice that is usually spontaneous parametric down-conversion (SPDC) in non-linear crystals, where a pump photon is, with a given probability, converted into a pair photons. The governing law for this process is momentum conservation that ensures correlations between the photons in the pair[16,17]. These correlations can be exploited for ghost imaging[18,19], imaging at enhanced spatial resolution[20,21], and to distil an image encoded in quantum states in the presence of classical background radiation[22,23]. A quantity of particular interest in quantum imaging is the spatial bi-photon joint probability distribution (JPD) describing the correlations between photon pairs. The reconstruction of the JPD can be achieved through statistical averaging over a large number of intensity images[24] – typically on the order of 10^6 to 10^7 images – of identically prepared photon pairs. Given that CCD based detectors provide frame rates on the order of 100 frames/s, the total acquisition time can vary from a few hours to over a day. Such long acquisition times constitute a hindrance to the widespread adoption of quantum imaging schemes for practical applications.

In the following, we show the reconstruction of the JPD in both position and momentum using a commercially available SPAD camera (SPC3, Micro Photon Devices). Correlation measurements in position and momentum space are averaged over a total of 10^7 images, amounting to an acquisition time of 140 s. These measurements are of a quality that allows to demonstrate spatial entanglement through violation of an Einstein-Podolsky-Rosen (EPR) criterion[25,26] with a confidence of 227 sigmas. We show an experimental study into the confidence of the violation as a function of the number of individual single-bit frames used for the calculation, highlighting the benefit of the high-frame rate enabled by the SPAD camera for fast characterisation of entanglement correlations. The short acquisition times required to reconstruct the bi-photon JPD paves the way for the implementation of quantum imaging schemes in real-time. Indeed, we note that faster sensors, with frame rates up to 800 kframes/s, have been demonstrated from other arrays[27] and that this work represents only the tip of the iceberg for the potential use of SPAD cameras within the field of quantum optics.

II. RESULTS

Figure 1 shows the experimental apparatus used to measure spatial correlations between photon pairs. Spatially entangled photon pairs are produced via spontaneous parametric down-conversion (SPDC) in a 0.5 mm long β-barium borate (BBO) crystal, cut for type-I phase matching. The crystal is pumped by a 347 nm pulsed laser with a repetition rate of 100 MHz (pulse length of 10 ns), an average power of 50 mW and is spatially filtered and collimated (not shown) to a beam diameter of 0.7 mm ($1/e^2$). Spectral filters block the pump beam and select near-degenerate photon pairs at 694 ± 5 nm. Photon pairs are detected using an MPD-SPC3 single-photon avalanche diode (SPAD) camera with an array of 32×64 pixels. The SPAD camera has a nominal speed of 96 kframes/s and is operated at its minimum exposure time (10 ns) and dead-time (50 ns). In Fig. 1a, the output surface of the crystal is imaged onto the SPAD camera using a $4f$-telescope; this configuration is used to measure position correlations of photons pairs on the surface of the BBO crystal (NF-configuration). To measure momentum correlations, we used another $4f$-telescope to image the Fourier plane of the BBO crystal surface onto the SPAD camera (FF-configuration), as shown in Fig. 1b.

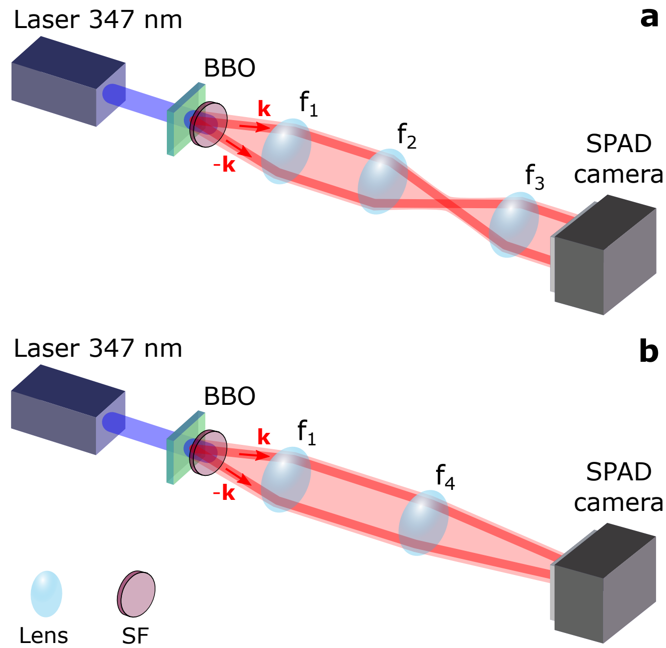

FIG. 1. **Experimental scheme.** Spatially-entangled photon pairs are produced by spontaneous parametric down-conversion (SPDC) in a β-barium borate (BBO) using a 347 nm pulsed pump laser with a repetition rate of 100 MHz. Spectral filters (SF) select near-degenerate photon pairs at 694 ± 5 nm. **a,** A three-lens system composed of $f_1 = 35$ mm, $f_2 = 100$ mm and $f_3 = 200$ mm, maps photons momenta onto pixels of a single-photon avalanche diode (SPAD) camera by Fourier imaging the crystal. This configuration is named FF-configuration. **b,** To measure position correlations, two lenses, $f_1 = 35$ mm and $f_4 = 300$ mm, image the output surface of the BBO crystal onto the SPAD camera. This configuration is named NF-configuration.

Measuring EPR entanglement. We demonstrate the presence of spatial entanglement in SPDC light by violating the Einstein-Podolsky-Rosen (EPR) criterion[26]

$$\Delta \mathbf{r} \cdot \Delta \mathbf{k} > \frac{1}{2}, \tag{1}$$

where $\Delta \mathbf{r} = \Delta(\mathbf{r_1} - \mathbf{r_2})$ and $\Delta \mathbf{k} = \Delta(\mathbf{k_1} + \mathbf{k_2})$ are, respectively, measures of the correlation strength in position and momentum for a pair of photons labelled 1 and 2. Violation of a related EPR criterion has been achieved previously both in the case of scanning single-point detectors[26] and by full-field imaging using an electron-multiplying CCD (EMCCD) cameras[28,29].

To determine the strength of the transverse position and momentum correlations, we measure the spatial JPD of photon pairs in the two configurations described in Fig. 1 using the SPAD camera. For a given pair of pixels located at positions $\mathbf{r_i}$ and $\mathbf{r_j}$ of the sensor, an element of the JPD denoted $\Gamma(\mathbf{r_i}, \mathbf{r_j})$ represents the joint probability of detecting photon $\mathbf{i}$ of a pair at pixel $\mathbf{r_i}$ and photon $\mathbf{j}$ at pixel $\mathbf{r_j}$. $\Gamma(\mathbf{r_i}, \mathbf{r_j})$ is calculated from a set of N frames using the formula[30]

$$\Gamma(\mathbf{r_i}, \mathbf{r_j}) = \frac{1}{N} \sum_{l=1}^{N} I_l(\mathbf{r_i}) I_l(\mathbf{r_j}) - \frac{1}{N^2} \sum_{m,n=1}^{N} I_m(\mathbf{r_i}) I_n(\mathbf{r_j}), \tag{2}$$

where $I_l(\mathbf{r_i}) \in \{0, 1\}$ is a binary value returned by the SPAD camera at pixel $\mathbf{r_i}$ in the l^{th} frame. The left term of the subtraction is an average value of the coincidence detection of photons belonging to either the same entangled pair (genuine coincidence) or different entangled pairs (accidental coincidence). Since multiple photon pairs can be detected during the time of an exposure, the contribution of accidental coincidences is generally greater than the genuine ones. The second term is an average value of accidental coincidences. Therefore, a subtraction between these two terms leaves only an average value of genuine coincidences that is $\Gamma(\mathbf{r_i}, \mathbf{r_j})$ (see Methods).

Reconstruction of bi-photon correlations. Figure 2 shows results of JPD measurements performed in the FF-configuration to study momentum correlations. Fig-

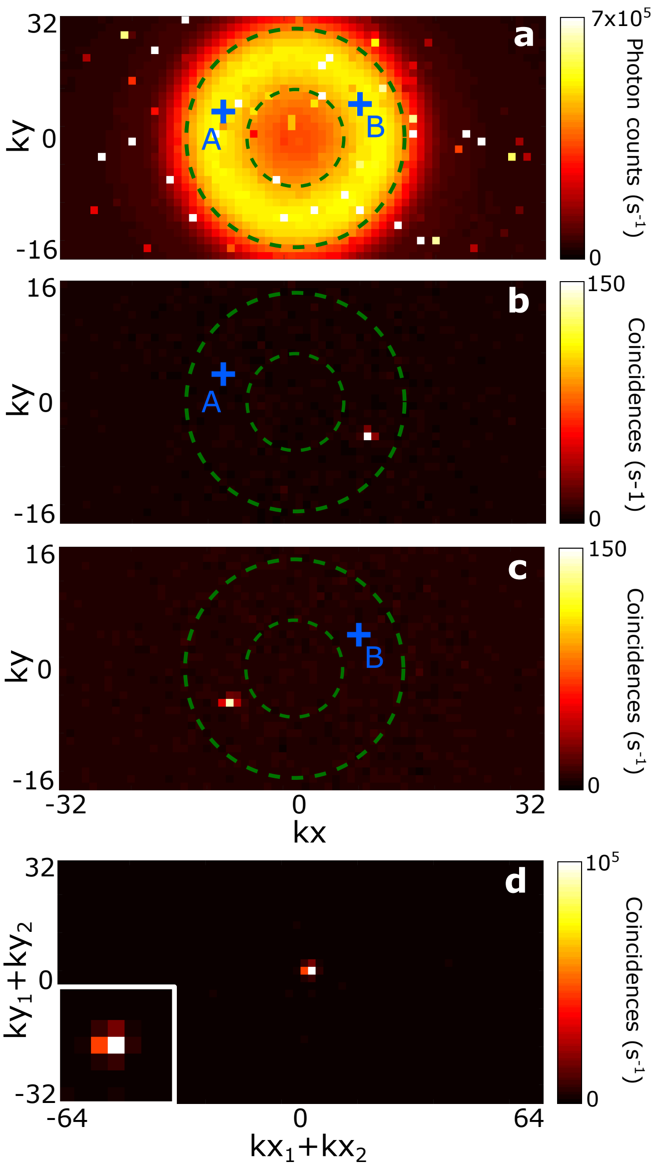

FIG. 2. **Measurement of momentum correlations. a,** Intensity distribution of the SPDC light measured in the FF-configuration. **b** and **c**, Conditional probability distributions $\Gamma(\mathbf{k}|\mathbf{A})$ and $\Gamma(\mathbf{k}|\mathbf{B})$ relative to two arbitrarily chosen positions **A** and **B** on the sensor, respectively. We measured an SNR of 320 (**b**) and 258 (**c**). **d**, Projection of the joint probability distribution (JPD) along the sum coordinates $\mathbf{k_1}+\mathbf{k_2}$. A measured momentum correlation width of $\Delta\mathbf{k} = 1.0666(7) \times 10^{-3}$ rad.μm^{-1} is obtained using a Gaussian fit (see Methods). Spatial coordinates are in pixels and the analysis was performed on a total of 10^7 images.

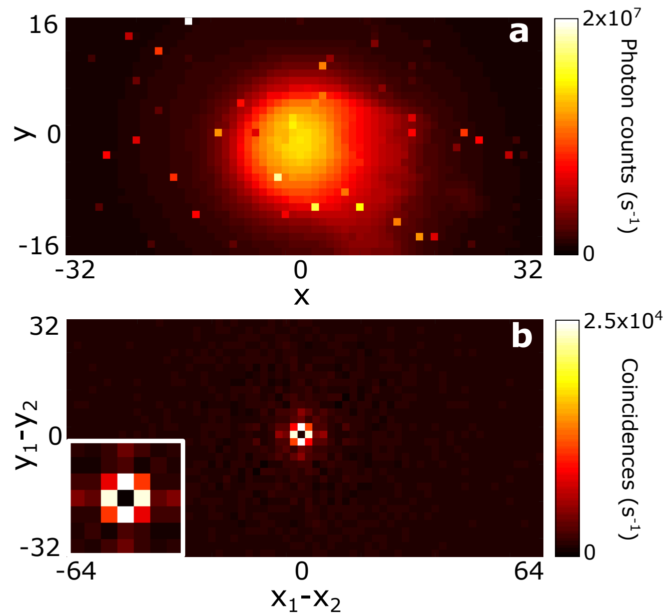

FIG. 3. **Measurement of position correlations. a,** Intensity distribution of the SPDC light in the NF-configuration. **b,** Projection of joint probability distribution along the minus-coordinates $\mathbf{r_1}-\mathbf{r_2}$. A measured position correlation width $\Delta\mathbf{r} = 4.3(2)$ μm was obtained using a Gaussian fit (see Methods). Spatial coordinates are in pixels and the analysis was performed on a total of 10^7 images.

ure 2a shows the direct intensity image reconstructed from the sum of 10^7 frames, which corresponds to a total acquisition time of 140 s. This image represents the probability of detecting a photon with a given momentum $\mathbf{k} = (k_x, k_y)$, with no information about the relative position of photons within the same pair (i.e. marginal probability distribution). The JPD $\Gamma(\mathbf{k_1}, \mathbf{k_2})$ is computed from this set of frames using Eq. 2 and is visualized using conditional projections. For example, Figs 2b and 2c show the conditional spatial distributions $\Gamma(\mathbf{k}|\mathbf{A})$ and $\Gamma(\mathbf{k}|\mathbf{B})$ of two photons measured by the sensor in coincidence and with high signal-to-noise ratio (SNR), with a one-photon detected at arbitrarily chosen positions **A** and **B**, respectively.

Due to momentum conservation in the SPDC process, the signal and idler photons are measured at π radians in the transverse plane at the center of the marginal distribution. The centrosymmetry of momentum correlations is characterised by the presence of an intense peak of coincidences in sum-coordinate projection of the JPD shown in Fig. 2d. The height of the peak corresponds to the sum of coincidences measured in all pairs of symmetric pixels, while its width gives the strength of the correlation, i.e., the momentum correlation width $\Delta\mathbf{k}$. Accounting for the effective magnification of our optical system, we measured $\Delta\mathbf{k} = 1.0666(7) \times 10^{-2}$ rad.μm^{-1} using a Gaussian fitting model (see Methods).

We repeated the above analysis in the NF-configuration shown in Fig. 1b to extract the position correlation width $\Delta\mathbf{r}$. The photons in entangled pairs are position correlated, i.e., they are born at the same position in the crystal and are expected to arrive at the SPAD sensor at the same position. Figures 3a and 3b show, respectively, the direct intensity image and the projection of the JPD along the minus-coordinate reconstructed from a set of 10^7 frames. A coincidence peak is observed at the center of the minus-coordinate projection that demonstrates strong position correlation between photon pairs. The central pixel in the minus-coordinate projection has been set to zero because the SPAD camera does not resolve the number of photons detected per pixel and therefore cannot measure photon coincidences at the same pixel. Accounting for the optical magnification, we measured a position correlation width $\Delta \mathbf{r} = 4.3(2)$ μm by fitting with a Gaussian model (see Methods).

The measured values of transverse position and momentum correlations width violate the EPR criterion in Eq. (1): $\Delta \mathbf{r} \cdot \Delta \mathbf{k} = 4.6(2) \times 10^{-2} < 1/2$, thus demonstrating the presence of spatial entanglement. This violation has a confidence level of $C = 227$ using the following definition:

$$C = \frac{|1/2 - \Delta \mathbf{r} \cdot \Delta \mathbf{k}|}{\sigma} \tag{3}$$

where $\sigma = 10^{-3}$ is the uncertainty on the product $\Delta \mathbf{r} \cdot \Delta \mathbf{k}$.

Confidence level analysis. As detailed in the Methods section, σ is calculated from the standard deviation of the noise surrounding the coincidence peaks in the sum- and minus-coordinates projections of the JPD. For a fixed exposure time and a constant source intensity, σ depends only on the number of frames acquired to compute the JPD[31]. Figure 4a shows that the measured values of C for different total number of frames N (black crosses) are found to scale as $\sqrt{N}$ (blue dashed curve, see Methods). In particular, confident EPR violation ($C > 5$) is not achieved for $N < 2 \times 10^4$. Figures 4b-g show examples of sum- and minus-coordinate projections obtained for a total number of frames $N = 2 \times 10^3$ (Figs 4b and 4e), $N = 10^4$ (Figs. 4c and 4f) and $N = 10^7$ (Figs. 4d and 4g). We clearly observe the decrease of the noise with the increase of the number of frames.

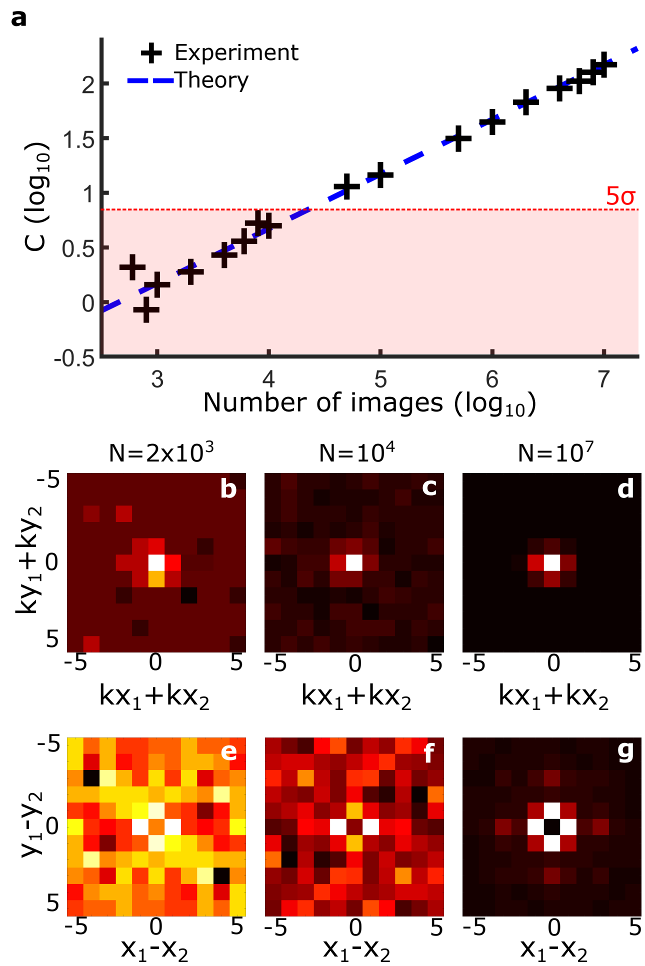

FIG. 4. **Confidence level analysis. a,** C values measured for different total number of frames N (black crosses) together with a theoretical model of the form $0.047\sqrt{N}$ (blue dashed line). **b-d**, Sum-coordinate projections of the JPD measured in the FF-configuration using **(b)** 2×10^3 frames, **(c)** 10^4 frames and **(d)** 10^7 frames. **e-g**, Minus-coordinate projection of the JPD measured in the NF configuration using **(e)** 2×10^3 frames, **(f)** 10^4 frames and **(g)** 10^7 frames.

III. DISCUSSION

We have used a SPAD camera to characterise the high dimensional correlations that arise from the spatial entanglement of photon pairs. By measuring position and momentum correlations using 10^7 intensity images, we showed a violation of an EPR criterion by 227 sigmas for an acquisition time of 140 s. While EPR violation has been demonstrated by acquiring very few frames with a highly-sensitive EMCCD camera[32], quantum imaging approaches based on correlation measurements between spatially entangled photon pairs require the measurement of a large number of frames[21–24,33,34], typically on the order of $10^6 - 10^7$. This is to ensure high enough SNR on the conditional projections to reconstruct the image by exploiting photon-pair correlations. Using an EMCCD for example, the reconstruction of the spatial JPD is performed at a frame rate of the order of 100 frames/s, amounting to a total acquisition time of many hours. Our ability to reduce the JPD measurement time by a factor of 1000× will allow quantum imaging proof-of-principle experiments to evolve towards practical applications.

IV. METHODS

Details on Γ reconstruction. Equation 2 enables the reconstruction of the spatial JPD from a finite number of frames N acquired with the SPAD camera. This equation is derived from a theoretical model of photon pair detection detailed in[30]. In this work, a link is established between the JPD and the measured frames at the limit

$N \to +\infty$:

$$\Gamma(\mathbf{r_i}, \mathbf{r_j}) = A \ln\left(1 + \frac{\langle I(\mathbf{r_i})I(\mathbf{r_j})\rangle - \langle I(\mathbf{r_i})\rangle\langle I(\mathbf{r_j})\rangle}{(1-\langle I(\mathbf{r_i})\rangle)(1-\langle I(\mathbf{r_i})\rangle)}\right), \tag{4}$$

where A is a constant coefficient that depends on both the quantum efficiency of the sensor and the power of the pump laser, and

$$\langle I(\mathbf{r_i})I(\mathbf{r_j})\rangle = \lim_{N\to+\infty} \frac{1}{N}\sum_{l=1}^{N} I_l(\mathbf{r_i})I_l(\mathbf{r_j}), \tag{5}$$

$$\langle I(\mathbf{r_i})\rangle = \lim_{N\to+\infty} \frac{1}{N}\sum_{l=1}^{N} I_l(\mathbf{r_i}). \tag{6}$$

Equation 4 is obtained under hypotheses[30] that are all verified in our work, including that (i) the quantum efficiency is the same for all pixels of the sensor and (ii) the number of pairs produced by SPDC during the time an exposure follows a Poisson distribution[35]. Moreover, in our experiment the probability of detecting a photon per pixel per frame is much lower than one ($\langle I(\mathbf{r})\rangle \ll 1$), which allows us to express Eq. 4 as follows:

$$\Gamma(\mathbf{r_i}, \mathbf{r_j}) \approx \langle I(\mathbf{r_i})I(\mathbf{r_j})\rangle - \langle I(\mathbf{r_i})\rangle\langle I(\mathbf{r_j})\rangle. \tag{7}$$

In the practical case where only a finite number of frames N is measured, the first term on the right-hand side in Eq. 7 is estimated by multiplying pixel values within the same frame:

$$\langle I(\mathbf{r_i})I(\mathbf{r_j})\rangle \approx \frac{1}{N}\sum_{l=1}^{N} I_l(\mathbf{r_i})I_l(\mathbf{r_j}). \tag{8}$$

The second term on the right-hand side in Eq. 7 is estimated by multiplying the averaged intensity values:

$$\langle I(\mathbf{r_i})\rangle\langle I(\mathbf{r_j})\rangle \approx \frac{1}{N^2}\sum_{m,n=1}^{N} I_m(\mathbf{r_i})I_n(\mathbf{r_j}). \tag{9}$$

Combining Eqs. 7, 8 and 9 finally leads to Eq 2.

$\Delta\mathbf{r}$ and $\Delta\mathbf{k}$ measurements and uncertainties. Transverse position and momentum correlation widths, $\Delta\mathbf{r}$ and $\Delta\mathbf{k}$, are estimated by fitting the sum- and minus-coordinate projections of the JPD measured in FF- and NF-configurations by a Gaussian model[28,29] of the form $a\exp(-r^2/2\Delta^2)$, where a is a fitting parameter and Δ is the desired correlation width value ($\Delta\mathbf{r}$ or $\Delta\mathbf{k}$). Note that, in the case of the position correlation width measurement, the central point of the minus-coordinate projection is excluded from the fitted data. The presence of noise in the sum- and minus-coordinate images induce uncertainties on values $\Delta\mathbf{r}$ and $\Delta\mathbf{k}$ returned by the fitting process. The standard deviation of the noise Σ is measured in an area composed of 40×40 pixels surrounding the central peak of coincidence. It relates to the correlation width uncertainty δ_Δ ($\delta_\Delta = \delta_{\Delta\mathbf{r}}$ or $\delta_{\Delta\mathbf{k}}$) through the error propagation equation

$$\delta_\Delta = \Sigma\sqrt{e}\Delta. \tag{10}$$

All correlation width values and uncertainties are expressed in the coordinate system of the crystal, after taking into consideration the magnifications introduced by the imaging systems detailed in Fig. 1.

Variation of the confidence level C with the number of images N. As defined in Eq. 3, the confidence levels C depends on both $\Delta\mathbf{r}\cdot\Delta\mathbf{k}$ and its uncertainty σ. For a given non-linear crystal and a stationary pump, $\Delta\mathbf{r}\cdot\Delta\mathbf{k}$ is constant while σ depends on the quality of our measurement, including the total number of acquired frames N. To establish the theoretical link between C and N, we first relate σ to the uncertainties in position and momentum correlation widths ($\delta_{\Delta\mathbf{r}}$ and $\delta_{\Delta\mathbf{k}}$) by error propagation:

$$\sigma = \Delta\mathbf{r}\cdot\Delta\mathbf{k}\sqrt{\left(\frac{\delta_{\Delta\mathbf{r}}}{\Delta\mathbf{r}}\right)^2 + \left(\frac{\delta_{\Delta\mathbf{k}}}{\Delta\mathbf{k}}\right)^2}. \tag{11}$$

Then, we replace $\delta_{\Delta\mathbf{k}}$ and $\delta_{\Delta\mathbf{r}}$ using Eq. 10 to show that $\sigma \propto \Sigma$. Finally, we use the fact that Reichert *et al.* have shown that $\Sigma \propto 1/\sqrt{N}$ for a constant average pump power and a fixed exposure time[31]. Thus, we conclude that $C \propto \sqrt{N}$. As shown in Fig. 4, this theoretical model fits successfully with the experimental data ($R^2 = 0.998$).

V. DATA AVAILABILITY

The experimental data and codes that support the findings presented here are available from the corresponding authors upon reasonable request.

---

* email: Bienvenu.Ndagano@glasgow.ac.uk

† email: Daniele.Faccio@glasgow.ac.uk

[1] A. Migdall, S. Polyakov, J. Fan, and J. Bienfang, Single-Photon Generation and Detection: Physics and Applications, Experimental methods in the physical sciences Elsevier, 2013.

[2] R. H. Hadfield, Nature Photonics **3**, 696 (2009).

[3] S. Cova, M. Ghioni, A. Lacaita, C. Samori, and F. Zappa, Applied Optics **35**, 1956 (1996).

[4] A. Rochas, M. Gani, B. Furrer, P. A. Besse, R. S. Popovic, G. Ribordy, and N. Gisin, Review of Scientific Instruments **74**, 3263 (2003).

[5] A. Rochas, M. Gosch, A. Serov, P. Besse, R. Popovic, T. Lasser, and R. Rigler, IEEE Photonics Technology Let-

ters **15**, 963 (2003).
[6] C. Bruschini, H. Homulle, I. M. Antolovic, S. Burri, and E. Charbon, Light: Science & Applications **8**, 87 (2019).
[7] D.-U. Li, J. Arlt, J. Richardson, R. Walker, A. Buts, D. Stoppa, E. Charbon, and R. Henderson, Optics Express **18**, 10257 (2010).
[8] R. K. Henderson, N. Johnston, H. Chen, D. D. U. Li, G. Hungerford, R. Hirsch, D. McLoskey, P. Yip, and D. J. Birch, ESSCIRC 2018 - IEEE 44th European Solid State Circuits Conference, 54 (2018).
[9] D. Bronzi, F. Villa, S. Tisa, A. Tosi, F. Zappa, D. Durini, S. Weyers, and W. Brockherde, IEEE Journal of Selected Topics in Quantum Electronics **20**, 354 (2014).
[10] I. Gyongy, T. Al Abbas, N. Finlayson, N. Johnston, N. Calder, A. Erdogan, N. W. Dutton, R. Walker, and R. K. Henderson, Emerging Imaging and Sensing Technologies for Security and Defence III; and Unmanned Sensors, Systems, and Countermeasures **10799**, 1079907 (2018).
[11] S. Lindner, C. Zhang, I. M. Antolovic, M. Wolf, and E. Charbon, 2018 IEEE Symposium on VLSI Circuits, 69 (2018).
[12] R. K. Henderson, N. Johnston, S. W. Hutchings, I. Gyongy, T. A. Abbas, N. Dutton, M. Tyler, S. Chan, and J. Leach, in IEEE International Solid-State Circuits Conference, 106 (2019).
[13] G. Gariepy, F. Tonolini, R. Henderson, J. Leach, and D. Faccio, Nature Photonics **10**, 23 (2016).
[14] A. Lyons, F. Tonolini, A. Boccolini, A. Repetti, R. Henderson, Y. Wiaux, and D. Faccio, Nature Photonics **13**, 575 (2019).
[15] G. Gariepy, N. Krstajić, R. Henderson, C. Li, R. R. Thomson, G. S. Buller, B. Heshmat, R. Raskar, J. Leach, and D. Faccio, Nature Communications **6**, 6021 (2015).
[16] B. M. Jost, A. V. Sergienko, A. F. Abouraddy, B. E. A. Saleh, and M. C. Teich, Optics Express **3**, 81 (1998).
[17] A. F. Abouraddy, M. B. Nasr, B. E. A. Saleh, A. V. Sergienko, and M. C. Teich, Physical Review A **63**, 063803 (2001).
[18] T. B. Pittman, Y. H. Shih, D. V. Strekalov, and A. V. Sergienko, Physical Review A **52**, R3429 (1995).
[19] P.-A. Moreau, E. Toninelli, T. Gregory, R. S. Aspden, P. A. Morris, and M. J. Padgett, Science Advances **5**, eaaw2563 (2019).
[20] D.-Q. Xu, X.-B. Song, H.-G. Li, D.-J. Zhang, H.-B. Wang, J. Xiong, and K. Wang, Applied Physics Letters **106**, 171104 (2015).
[21] E. Toninelli, P.-A. Moreau, T. Gregory, A. Mihalyi, M. Edgar, N. Radwell, and M. Padgett, Optica **6**, 347 (2019).
[22] H. Defienne, M. Reichert, J. W. Fleischer, and D. Faccio, Science Advances **5**, eaax0307 (2019).
[23] T. Gregory, P-A. Moreau, E. Toninelli, and M. J. Padgett, Science Advances (in press) arXiv:1907.09370v1 (2019).
[24] M. Reichert, H. Defienne, and J. W. Fleischer, Scientific Reports **8**, 7925 (2018).
[25] A. Einstein, B. Podolsky, and N. Rosen, Physical Review **47**, 777 (1935).
[26] J. C. Howell, R. S. Bennink, S. J. Bentley, and R. W. Boyd, Physical Review Letters **92**, 210403 (2004).
[27] L. Gasparini, M. Zarghami, H. Xu, L. Parmesan, M. M. Garcia, M. Unternhrer, B. Bessire, A. Stefanov, D. Stoppa, and M. Perenzoni, 2018 IEEE International Solid-State Circuits Conference - (ISSCC), 98 (2018).
[28] P.-A. Moreau, J. Mougin-Sisini, F. Devaux, and E. Lantz, Physical Review A **86**, 010101 (2012).
[29] M. Edgar, D. Tasca, F. Izdebski, R. Warburton, J. Leach, M. Agnew, G. Buller, R. Boyd, and M. Padgett, Nature Communications **3**, 984 (2012).
[30] H. Defienne, M. Reichert, and J. W. Fleischer, Physical Review Letters **120**, 203604 (2018).
[31] M. Reichert, H. Defienne, and J. W. Fleischer, Physical Review A **98**, 013841 (2018).
[32] E. Lantz, S. Denis, P.-A. Moreau, and F. Devaux, Optics Express **23**, 26472 (2015).
[33] H. Defienne, M. Reichert, and J. W. Fleischer, Physical Review Letters **121**, 233601 (2018).
[34] H. Defienne, B. Ndagano, A. Lyons, and D. Faccio, arXiv:1911.01209 (2019).
[35] T. S. Larchuk, M. C. Teich, and B. E. A. Saleh, Annals of the New York Academy of Sciences **755**, 680 (1995).

VI. ACKNOWLEDGEMENTS

D.F. acknowledges financial support from the UK Engineering and Physical Sciences Research Council (grants EP/M01326X/1 and EP/R030081/1) and from the European Union's Horizon 2020 research and innovation programme under grant agreement No 801060. H.D. acknowledges financial support from the EU Marie-Curie Sklodowska Actions (project *840958*).

VII. AUTHORS CONTRIBUTIONS

B.N. performed the experiment. B.N. and H.D. analysed the results. B.N., H.D., A.L. and D.F. conceived and discussed the experiment. F.V. and S.T. provided experimental support with the SPAD camera. All authors contributed to the redaction of the manuscript.

VIII. COMPETING INTERESTS

The authors declare no competing interests.